Supporting Information

Tapley et al. 10.1073/pnas.0811811106

SI Materials and Methods

HdeA Purification. HdeA protein was expressed from BL21(DE3) cells harboring the plasmid pET21a-hdeA. Three 1-L cultures were grown to midlog phase (A_{600} ≈1), and protein expression was induced by the addition of IPTG to a final concentration of 0.3 mM. Cells were grown for an additional 4 h and harvested by centrifugation. Periplasmic extracts were prepared by resuspending the cell pellets in 60 mL of 50 mM Tris buffer at pH 7.5 containing 50 mM NaCl and 1 mg/mL polymyxin sulfate (1), swirling for 1 h at 4 °C, and centrifuging for 20 min at 15,000 × *g* to remove the cytoplasmic fraction and cell debris. These extracts were then dialyzed overnight against 20 mM Tris, 0.5 mM ETDA (pH 8) and filtered (0.2-μm pore) before protein was loaded onto a Hi-Trap Q–Sepharose anion exchange column (GE Healthcare). HdeA was eluted with a linear gradient from 0 to 0.5 M NaCl in 20 mM Tris, 0.5 mM ETDA (pH 8). Fractions containing HdeA were pooled and dialyzed overnight against 20 mM acetate buffer with 0.5 mM EDTA (pH 4.0). The pool was then filtered (0.2-μm pore) and loaded onto a Hi-Trap SP–Sepharose cation exchange column (GE Healthcare) and eluted with a linear 0–1 M NaCl gradient in 20 mM acetate, 0.5 mM EDTA (pH 4.0). Fractions containing HdeA were pooled, concentrated to ≈500 μM, and flash-frozen in liquid nitrogen.

HdeA variants were constructed by using the QuikChange site-directed mutagenesis technique (Stratagene) with the plasmids pET21a-*hdeA* or pET21a-*hdeA*-W16F/W82L as templates (see Table S1 for a summary of HdeA mutants and nomenclature used in the text). The HdeA variants were expressed and purified as described for wild-type HdeA, with the exception that protein expression was conducted in a *hdeA*-null strain (BL21 kan::*hdeA*) to exclude contamination by wild-type HdeA. The chromatographic behavior, far-UV circular dichroism (CD) spectra, and chaperone activity of each mutant were similar to those of wild-type HdeA, indicating that the mutations introduced did not grossly alter protein structure (Fig. S10).

HdeA Activity Assays. Aggregation assays were performed by diluting Gdn-denatured rhodanese to a final concentration of 4 μM into 100 mM phosphate buffer, 150 mM NaCl (pH 2.2), in the absence or presence of 4 μM HdeA. Aggregation was monitored by following absorbance at 320 nm in a Cary100 spectrophotometer equipped with a Peltier temperature control unit set to 37 °C. Malate dehydrogenase (MDH) denaturation and aggregation assays were performed as described for rhodanese except that 150 mM ammonium sulfate was added to the aggregation buffer to facilitate MDH aggregation.

CD. CD measurements were recorded with a Jasco J-810 spectropolarimeter. Far-UV CD spectra (190–250 nm) were recorded by using 10 μM solutions of HdeA in 10 mM phosphate buffer at the indicated pH in quartz cuvettes with a path length of 0.1 cm. Near-UV CD spectra (260–310 nm) were recorded by using 85 μM HdeA in 10 mM phosphate buffer at the indicated pH in quartz cuvettes with a path length of 1 cm.

Curve Fitting for Determination of K_d Values. Fluorescence intensity at 350 nm for wild-type HdeA, or 330 nm for HdeA(W35), was measured and plotted as a function of MDH concentration. Because we observed tight binding of MDH such that the free (i.e., unbound) MDH concentration was not accurately represented by the total MDH concentration, we fit the binding isotherms by using the equation

$$F = F_b/2\{K_d + S_0 + nE_0 - [(K_d + S_0 + nE_0)^2 - 4nE_0S_0]^{1/2}\} + F_f(E_0 - 0.5\{K_d + S_0 + nE_0 - [(K_d + S_0 + nE_0)^2 4nE_0S_0]^{1/2}\}) \quad [s1]$$

where F is the observed fluorescence, F_b is the fluorescence of substrate-bound HdeA, F_f is the fluorescence of free HdeA, S_0 is the total MDH concentration, E_0 is the total HdeA concentration, and n is the number of binding sites.

Fluorescence Labeling and FRET Measurements. Labeling of HdeA(C27) was performed by first reducing Cys-27 in 20 mM Tris buffer, 10 mM DTT (pH 8) on ice for 1 h. The intrinsic Cys-16–Cys-66 disulfide of HdeA is buried and unaffected by DTT treatment under these conditions, as evidenced by fluorescence emission spectra. Excess DTT was removed with a NAP5 desalting column (GE Healthcare). HdeA was then incubated with a 10-fold molar excess of either monobromobimane or Alexa Fluor 532 (AF532; C-5 maleimide) dye in 50 mM Tris buffer, 50 mM NaCl (pH 8) for 1 h at 25 °C. Excess dye was removed with NAP5 desalting columns. For HdeA labeled with bimane or AF532, labeling efficiency was determined spectrophotometrically by comparing the absorbance of the dye (bimane, ε_{380} = 5,000 M^{-1} cm^{-1}, ε_{280} = 3,600 M^{-1} cm^{-1}; AF532, ε_{528} = 78,000 M^{-1} cm^{-1}, ε_{280} = 7,290 M^{-1} cm^{-1}) to the absorbance of unlabeled HdeA (ε_{280} = 11,200 M^{-1} cm^{-1}). Label-to-protein ratios between 0.8 and 0.9 were observed, indicating specific labeling of Cys-27.

For intermolecular FRET measurements, heterodimers of HdeA(C27)-bimane and HdeA(C27)-AF532 were formed by first mixing relatively high concentrations (50 μM) of each labeled protein in 100 mM phosphate (pH 2.2) and subsequently adding small aliquots (typically 10 μL) of this mixture into 1 mL of neutral pH phosphate buffer for a final concentration of highly FRET-efficient mixed labeled dimers of 1 μM. Emission spectra were recorded from 400 to 700 nm by using λ_{ex} of 390 nm (slit widths, 5 nm). Stopped-flow FRET measurements were recorded by using λ_{ex} of 390 nm and a 550-nm long-pass emission filter; other conditions were identical to those described for tryptophan fluorescence measurements.

For intramolecular FRET measurements, emission spectra of 1 μM trinitrobenzoic acid (TNB)-labeled HdeA(W82,C27) were recorded from 290 to 420 nm (λ_{ex} = 280 nm) at either pH 7 or pH 2.2. For measurements at pH 7, mixed dimers between HdeA(W82,C27)-TNB and tryptophan-free HdeA(W16F/W82L) were formed by incubating HdeA(W82,C27)-TNB with a 5-fold molar excess of Trp-less HdeA at pH 2.2 for 1 min before neutralizing the solution. This was done to eliminate unwanted intermolecular FRET from occurring between adjacent monomers within the HdeA dimer (e.g., W82′ to C27-TNB or W82 to C27′-TNB). To test the effects of substrate binding, the same assays were conducted at pH 2.2 in the presence of 4 μM ADH, rhodanese, or MDH, each of which was treated with *N*-bromosuccinimide (NBS). NBS treatment was performed to eliminate unwanted intrinsic tryptophan and tyrosine fluorescence by the substrate proteins (2, 3). Each substrate was incubated in 200 μM NBS for 1 min, followed by the addition of L-methionine to a final concentration of 10 mM to quench excess NBS.

For distance calculations, emission spectra were recorded as above except that the TNB label was cleaved by adding a small amount of solid DTT to the solution. FRET efficiency (E_T) was

then calculated by using the integrated fluorescence intensities of the tryptophan donor in the absence (F_D) and presence (F_{DA}) of the TNB acceptor according to the equation

$$E_T = 1 - F_{DA}/F_D \quad \textbf{[s2]}$$

E_T was then used to calculate the apparent distance (r) by using the equation

$$r = R_0*[(1 - E_T)/(E_T)]^{1/6} \quad \textbf{[s3]}$$

The Förster distance (R_0) of the tryptophan (donor) and TNB (acceptor) pair was determined as described in the following section.

Fluorescence Quantum Yield and R_0 Determination. The Förster distance (R_0) of the tryptophan (donor) and TNB (acceptor) pair has been reported by Wu and Brand (4) to be 24.5 Å. However, R_0 is sensitive to changes in donor quantum yield (5), so we first needed to determine the quantum yield of Trp-82 of HdeA under various conditions (pH 7, pH 2.2, and 5 M Gdn) and the resulting changes in R_0. We also needed to calculate R_0 for the W82-AF350 pair and the bimane-AF532 pair. We determined quantum yields (Q) for each donor probe according to the technical article "A guide to recording fluorescence quantum yields" provided by Jobin Yvon, using either *N*-acetyltryptophanamide (NATA) in water ($Q = 0.14$) or bimane in water ($Q = 0.23$) as reference solutions. The resulting quantum yields for HdeA(W82) were 0.23 at pH 7, 0.065 at pH 2.2, and 0.095 in 5 M Gdn, and 0.33 for C27-bimane at pH 2.2. R_0 values were then calculated according to the equation

$$R_0 = 0.211[\kappa^2 n^{-4} Q_D J(\lambda)]^{1/6} \quad \textbf{[s4]}$$

where Q_D is the quantum yield of the donor in the absence of acceptor, n is the refractive index of the solvent (a value of 1.33 for aqueous buffers was used in all calculations), and κ^2 is the dipole orientation factor (a dynamic average value of 2/3 was used in all calculations; this value was deemed a reasonable approximation according the fast anisotropy decay of the W82 donor and AF350 acceptor in the absence and presence of bound substrate; see Fig. S9). $J(\lambda)$ is the spectral overlap integral of donor emission and acceptor absorbance, defined as

$$J(\lambda) = \int f_D(\lambda)\varepsilon_A(\lambda)\lambda^4 d\lambda \quad \textbf{[s5]}$$

where f_D is the normalized donor emission spectrum and ε_A is the molar extinction coefficient of the acceptor at wavelength λ. Extinction coefficients of 8,890 M^{-1} cm^{-1} for TNB (at 324 nm), 17,000 M^{-1} cm^{-1} for AF350 (at 345 nm), or 78,000 M^{-1} cm^{-1} for AF532 (at 528 nm) were used to calculate the following R_0 values in each environment:

Donor	Acceptor	R_0 (pH 7)	R_0 (pH 2.2)	R_0 (5 M Gdn)
W82	C27-TNB	25.2 ± 0.6 Å	20.4 ± 0.5 Å	21.8 ± 0.5 Å
W82	C27-AF350	30.4 ± 0.8 Å	24.6 ± 0.6 Å	ND
C27-bimane	C27-AF532	ND	52.2 ± 1.3 Å	ND

Determination of R_0 values required the measurement of donor quantum yield (Q_D), normalized donor emission spectrum (f_D), and molar extinction coefficient of the acceptor (ε_A) under different conditions. Assuming an error of ±5% in each of these individual measurements resulted in the reported error for each R_0. ND, not determined.

Assessment of Uncertainty Associated with Reported Distances. Uncertainties in the reported donor–acceptor distances obtained by steady-state emission spectra were estimated as follows. First, triplicate measurements of three independent samples were recorded (i.e., the emission spectra in Fig. 5), and SD values in the integrated fluorescence intensity and the resulting transfer efficiency were determined. The average value for donor to acceptor transfer efficiency (E_T) was then distorted by either +1 or −1 SD based on the triplicate measurements. The resulting smaller values of E_T (E_T − 1 SD) were then used to calculate distances with the minimal estimated values of R_0 reported in the preceding table; the larger values of E_T (E_T +1 SD) were used with the maximal estimated values of R_0 such that uncertainties in R_0 were propagated into distance calculations. The differences between the minimum and maximum distances calculated in this way correspond to the errors reported in the text.

Fluorescence Lifetime Measurements. Time-correlated single-photon measurements (TCSPC) were carried out by using standard procedures (6) in reverse counting mode. A Coherent Verdi V-10 diode laser pumped a Coherent model Mira 900 Ti;sapphire laser operating with a pulse width of 150 fs. The output was frequency-tripled to 283 nm by using an Inrad model 5-050 ultrafast harmonic generating system. The excitation rate was 4 MHz and was controlled by a Coherent 9200 Pulse Picker. Fluorescence emission was detected with a Hamamatsu R3809U-50 microchannel plate photomultiplier connected to a Tennelec quad constant fraction discriminator (model TC455). Analog output from an Ortec time–amplitude converter (model 457) was digitized by an in-house system built from National Instruments hardware (NI6070 12-bit A/D converter, NI6602 counter) and controlled by Labview software. The samples contained 1 μM HdeA(W82,C27) in the absence or presence of the TNB quencher attached via C27. For experiments in the presence of MDH, the final concentration was 2 μM. Lifetime distributions were determined by using a maximum entropy method algorithm. In most cases, multiple distinct lifetimes were observed, which is likely because of different tryptophan rotamers. Lifetimes of the separate rotamer populations in the absence (τ_D) or presence of acceptor (τ_{DA}) or the lifetimes obtained by combining the two rotamer peaks into an average lifetime (τ_{av}) were then used to calculate transfer efficiency (E_T) and apparent distances (r) according to the Equation s3 and

$$E_T = 1 - \tau_{DA}/\tau_D \quad \textbf{[s6]}$$

1. Dixon RA, Chopra I (1986) Leakage of periplasmic proteins from *Escherichia coli* mediated by polymyxin B nonapeptide. *Antimicrobial Agents Chemother* 29:781–788.
2. Ohnishi M, Kawagishi T, Abe T, Hiromi K (1980) Stopped-flow studies on the chemical modification with *N*-bromosuccinimide of model compounds of tryptophan residues. *J Biochem* 87:273–279.
3. Spande TF, Green NM, Witkop B (1966) The reactivity toward *N*-bromosuccinimide of tryptophan in enzymes, zymogens, and inhibited enzymes. *Biochemistry* 5:1926–1933.
4. Wu P, Brand L (1994) Conformational flexibility in a staphylococcal nuclease mutant K45C from time-resolved resonance energy transfer measurements. *Biochemistry* 33:10457–10462.
5. Lakowicz JR (2006) *Principles of Fluorescence Spectroscopy* (Springer, New York).
6. O'Connor DV, Phillips D (1984) *Time-Correlated Single Photon Counting* (Academic, London).
7. Gajiwala KS, Burley SK (2000) HDEA, a periplasmic protein that supports acid resistance in pathogenic enteric bacteria. *J Mol Biol* 295:605–612.

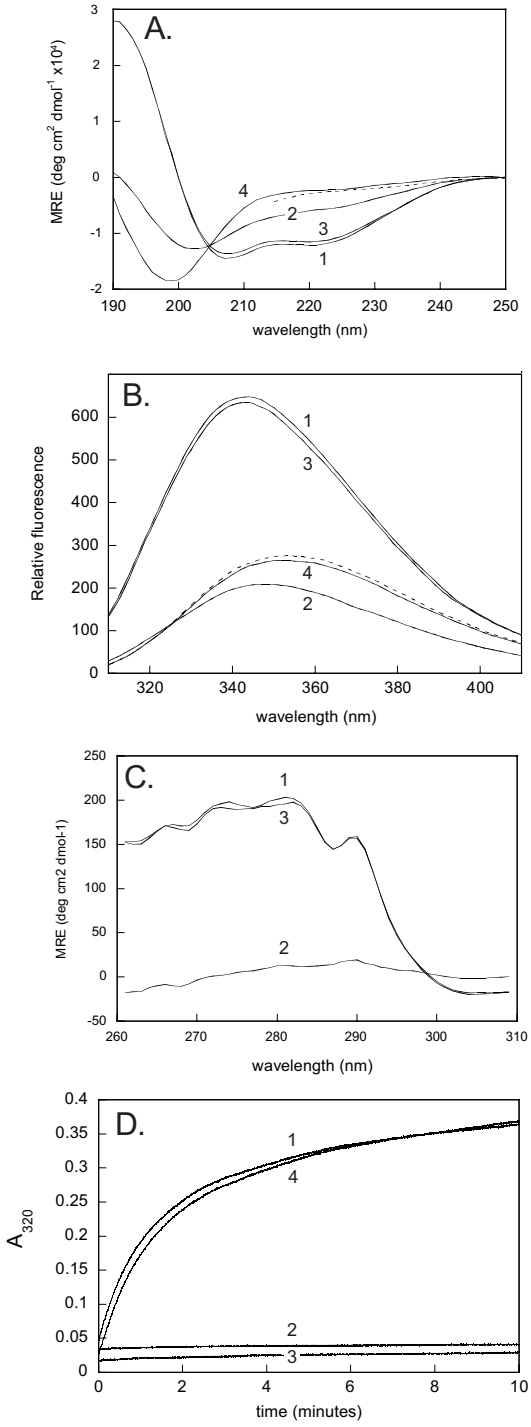

Fig. S1. HdeA retains structure at low pH, which is necessary for chaperone activity. (*A*) Far-UV CD spectra of 10 μM $HdeA_{pH7.0}$ (trace 1), $HdeA_{pH2.2}$ (trace 2), neutralized $HdeA_{pH2.2\Rightarrow7.0}$ (trace 3), heat-treated and reduced $HdeA_{red}$ (trace 4), and fully denatured HdeA in 5 M Gdn (dashed line). The spectrum of reduced HdeA is very similar to that taken in 5 M Gdn, indicating that reduced HdeA is completely unfolded. However, this spectrum is quite different from that of active HdeA at pH 2.2, indicating a significant degree of residual structure in active $HdeA_{pH2.2}$. Spectra are plotted as mean residue ellipticity (MRE) versus wavelength. (*B*) Fluorescence emission spectra of 5 μM $HdeA_{pH7.0}$ (trace 1), $HdeA_{pH2.2}$ (trace 2), neutralized $HdeA_{pH2.2\Rightarrow7.0}$ (trace 3), heat-treated and reduced $HdeA_{red,\ pH\ 7.0}$ (trace 4), and fully denatured $HdeA_{Gdn}$ (dashed line) are shown. (*C*) Near-UV CD spectra of 85 μM $HdeA_{pH7.0}$ (trace 1), $HdeA_{pH2.2}$ (trace 2), and neutralized $HdeA_{pH2.2\Rightarrow7.0}$ (trace 3) suggest that HdeA reversibly loses tertiary structure at low pH. (*D*) HdeA Cys-18–Cys-66 disulfide bond is required for chaperone activity. Gdn-denatured rhodanese was diluted to a final concentration of 4 μM into pH 2.2 buffer in the absence (1) or presence of 4 μM untreated HdeA (2), 4 μM HdeA that was unfolded in 5 M Gdn before dilution into the assay buffer (3), or 4 μM HdeA that was unfolded in 5 M Gdn in the presence of 10 mM DTT before dilution into the assay buffer (4). The treatment in (4) leads to the cleavage of the Cys-18–Cys-66 disulfide bond, which inactivates HdeA. Assays were performed in 100 mM potassium phosphate, 150 mM NaCl (pH 2.2) at 37 °C. Aggregation was monitored by the apparent absorbance increase at 320 nm caused by light scatter.

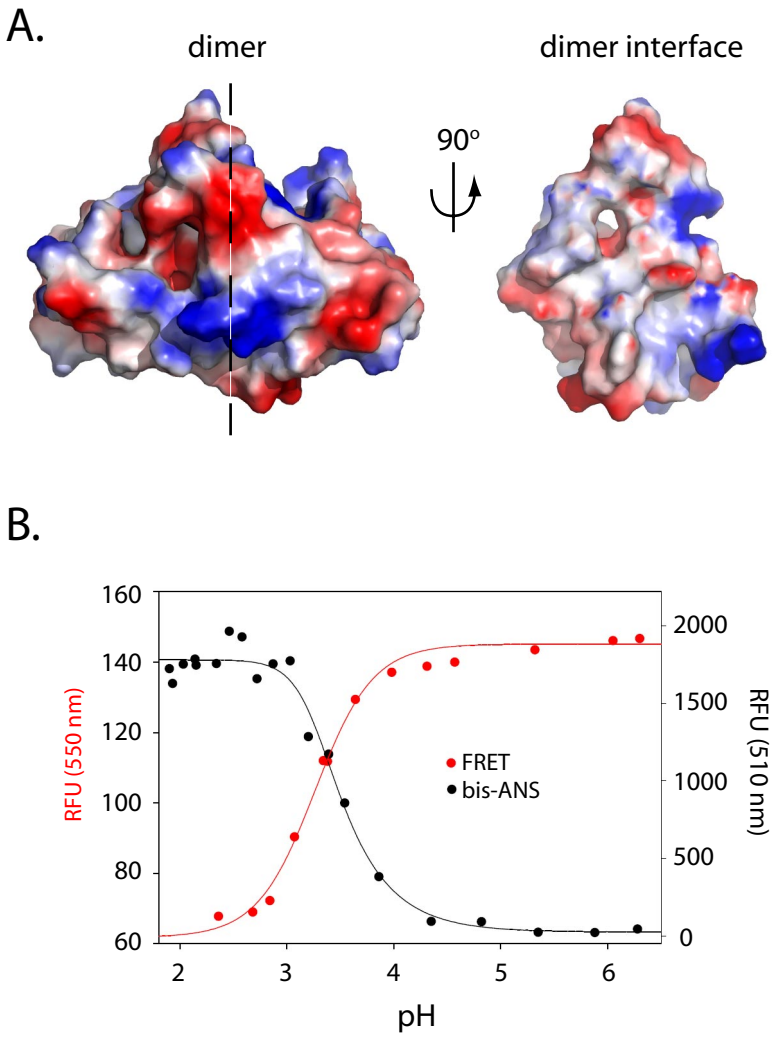

Fig. S2. HdeA monomerization results in exposure of hydrophobic surfaces that bind the fluorescent dye bis-ANS. (*A*) (*Left*) Electrostatic surface representation of the HdeA dimer reveals a highly charged molecule. (*Right*) Removal of one HdeA monomer, and rotation by 90° reveals a dimer interface that is largely hydrophobic. Representations were generated in PyMol (Delano Scientific) by using chains A and B from PDB ID code 1DJ8 (7). The approximate dimer interface is demarcated by a dashed line. (*B*) The pH transition midpoints for monomerization (as monitored by FRET) and exposure of hydrophobic surfaces (as monitored by bis-ANS binding) coincide. The binding of bis-ANS was monitored by mixing 4 μM HdeA and 20 μM bis-ANS in 10 mM citrate buffer, 150 mM NaCl, and then titrating the pH from ≈6.5 to 2 by small, stepwise additions of 0.5 M HCl. The compound bis-ANS is essentially nonfluorescent in aqueous buffers unless it is bound to a hydrophobic surface such as a partially unfolded protein, and the bis-ANS fluorescence increases as HdeA unfolds at low pH. FRET experiments were performed in the same buffer, starting with 1 μM mixed bimane- and AF532-labeled HdeA(S27C) dimers and titrating the pH from ≈6.5 to 2. The decrease in fluorescence at 550 nm at low pH is caused by HdeA monomerization, which leads to decreased FRET efficiency.

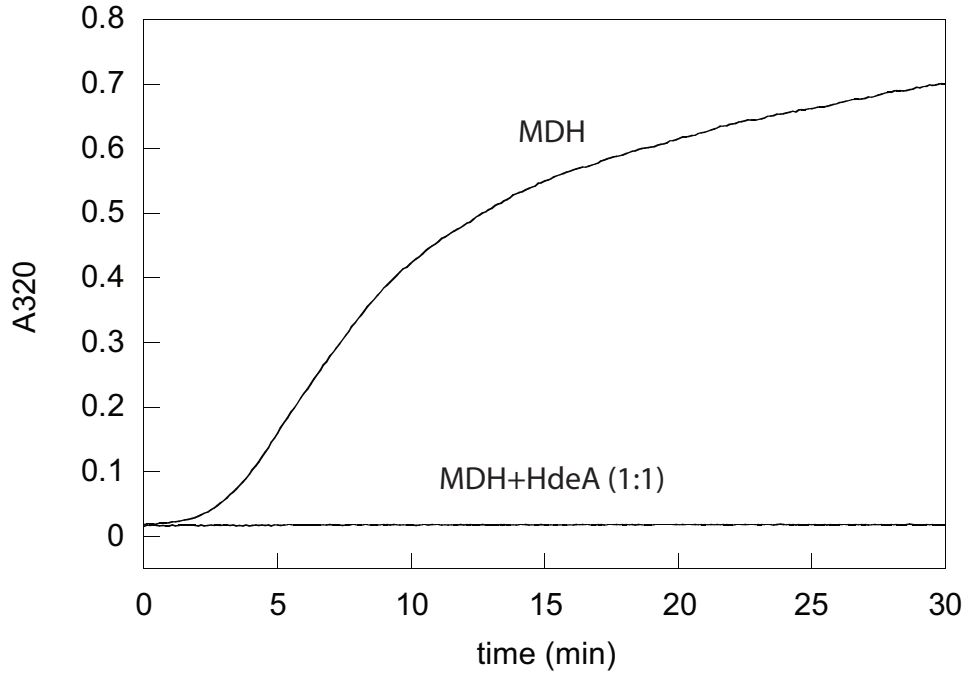

Fig. S3. HdeA efficiently suppresses aggregation of the model substrate MDH. Gdn-denatured MDH was diluted to a final concentration of 8 μM into 100 mM phosphate buffer (pH 2.2) containing 150 mM NaCl and 150 mM ammonium sulfate in the absence or presence of 8 μM HdeA. Aggregation was monitored at 37 °C by following apparent absorbance changes at 320 nm caused by light scatter.

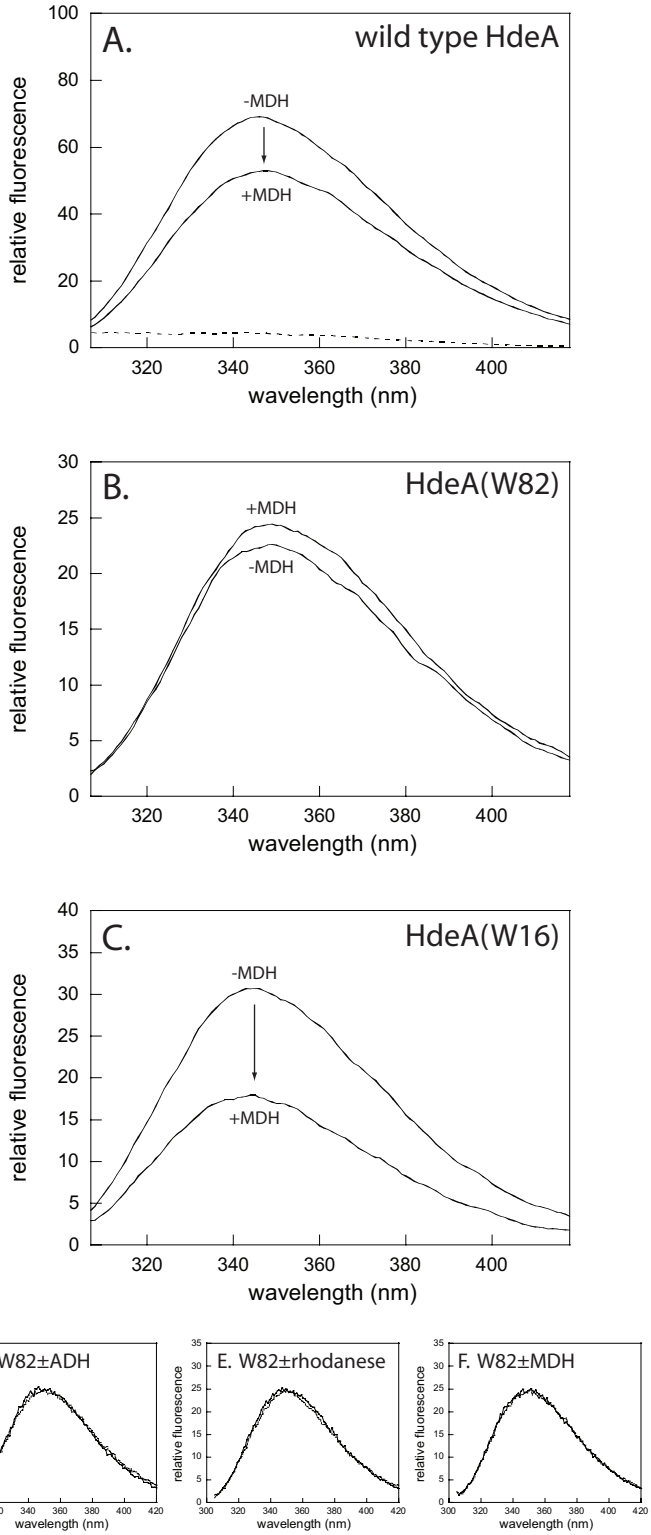

Fig. S4. The effect of MDH binding on HdeA tryptophan fluorescence is caused by interactions with W16. (*A*–*C*) Tryptophan emission spectra. One micromolar wild-type HdeA (*A*), HdeA(W82) (*B*), and HdeA(W16) (*C*), each in the absence or presence of 2 μM MDH. (*D*–*F*) Emission spectra of 1 μM HdeA(W82) in the absence (solid line) or presence (dashed line) of 2 μM NBS-treated ADH (*D*), NBS-treated rhodanese (*E*), or NBS-treated MDH (*F*). The addition of NBS-treated substrates resulted in 0.4%, 2%, and 0.7% decreases in the total observed fluorescence intensity, respectively. Emission spectra were recorded in 100 mM phosphate buffer, 150 mM NaCl (pH 2.2) with an excitation wavelength of 295 nm. The dashed line in *A* is the spectrum of 2 μM MDH alone.

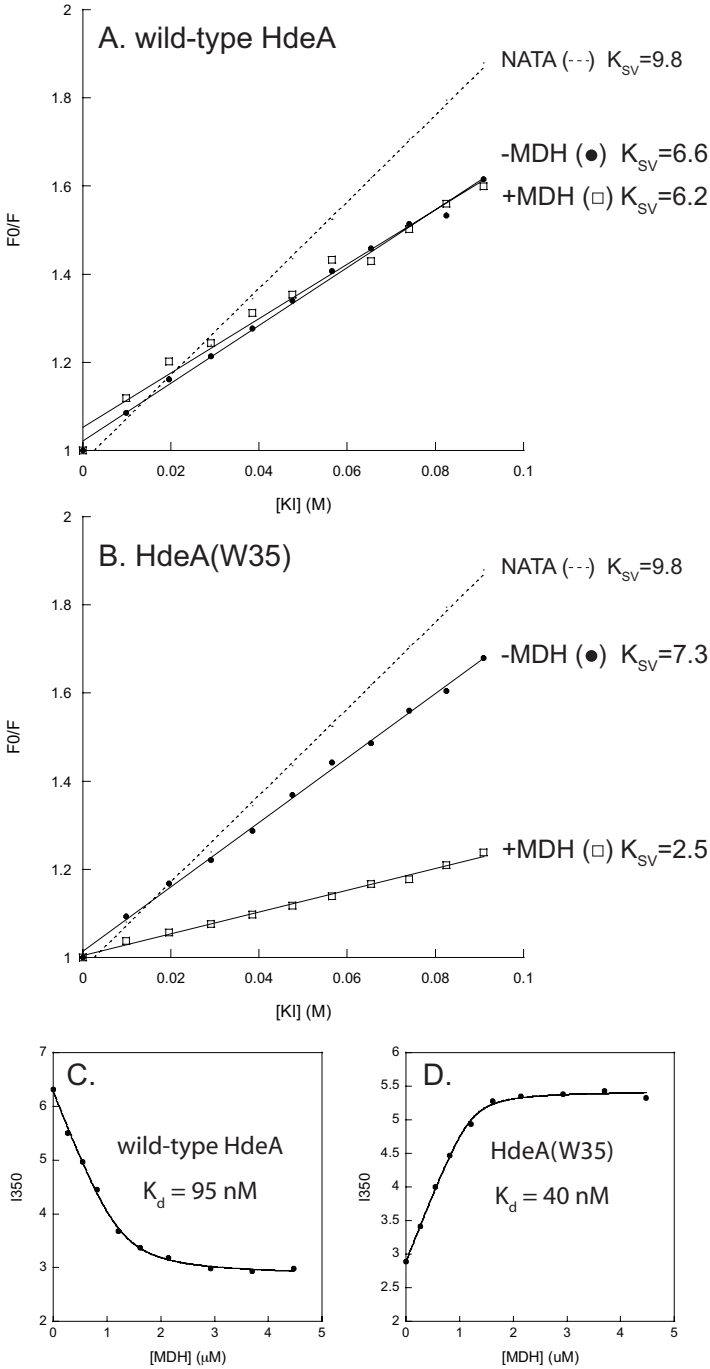

Fig. S5. MDH binding causes significant burial of tryptophan at position 35 but does not affect solvent exposure of tryptophan 16 or 82. (*A* and *B*) Stern–Volmer plots for potassium iodide (KI) quenching of wild-type HdeA (*A*) and HdeA(W35) (*B*) in the absence or presence of bound MDH are shown. Emission spectra (305–420 nm, 5-nm band pass) were collected by using an excitation wavelength of 295 nm (5-nm band pass) of 1 μM HdeA in the absence or presence of 2 μM MDH in 100 mM potassium phosphate, 150 mM NaCl (pH 2.2). Spectra were corrected and integrated, which yielded the fluorescence intensity in the absence of quencher (F_0). Spectra were then recorded following stepwise, 10-μL additions of 1 M KI. All spectra were corrected for dilution and Raman scatter to yield the fluorescence intensity (F) in the presence of a given concentration of quencher. Spectra were also corrected for a minimal fluorescence component caused by MDH, where appropriate. F_0/F was plotted against KI concentration and fit by linear regression to determine the slope, which is equal to the Stern–Volmer quenching constant (K_{SV}). Traces for NATA, which represents a maximally solvent-exposed tryptophan (K_{SV} = 9.8), are shown as dashed lines for comparison. (*C* and *D*) MDH-binding wild-type HdeA (*C*) and HdeA(W35) (*D*) in the presence of 150 mM NaCl + 100 mM KCl. The titrations presented in the *Insets* of Fig. 4 were performed in 150 mM NaCl, which resulted in similar apparent K_d values; therefore the change in ionic strength caused by the addition of KI in *A* and *B* should not significantly perturb the HdeA–MDH interaction.

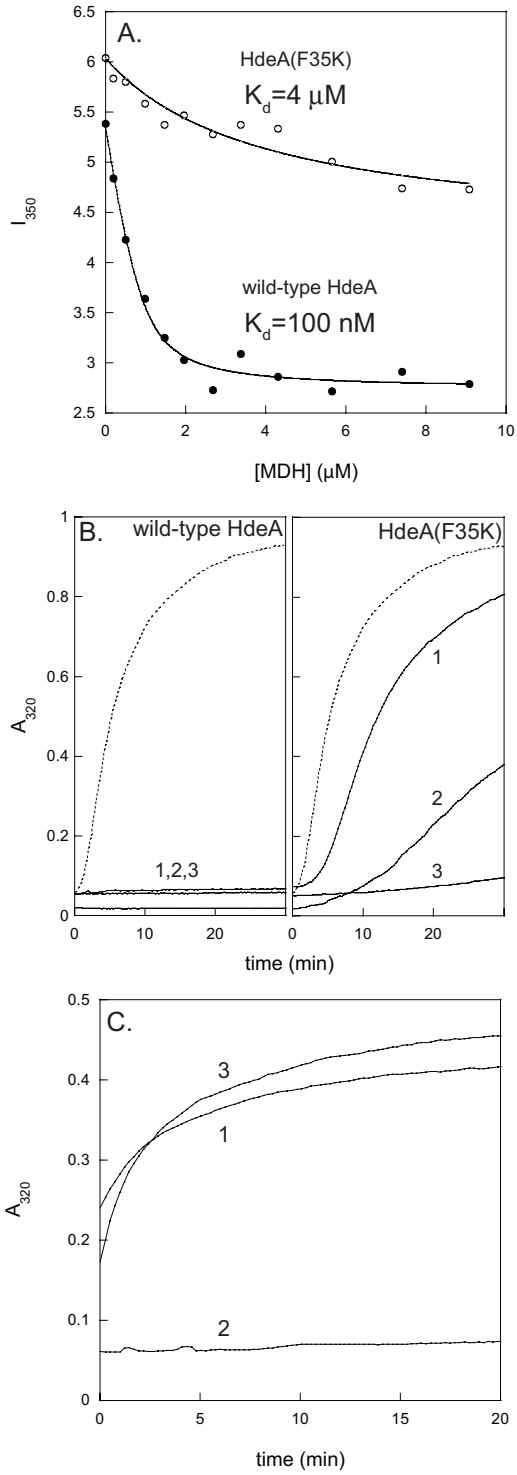

Fig. S6. Introduction of a charged residue at the dimer interface of HdeA results in a dramatic reduction in substrate binding affinity and severely impaired chaperone activity. (*A*) Titrations of MDH into solutions of 1 μM wild-type HdeA (filled circles) or 1 μM HdeA(F35K) (open circles). Emission spectra were recorded in the absence or presence of increasing amounts of MDH; the corrected peak intensities at 350 nm were plotted versus MDH concentration and fit to obtain K_d values of 100 nM for wild-type HdeA and 4 μM for HdeA(F35K). (*B*) Aggregation of Gdn-denatured MDH (8 μM final concentration) in the absence (dashed line) or presence of wild-type HdeA (*Left*) or HdeA(F35K) (*Right*) as monitored by absorbance at 320 nm. Final HdeA concentrations in both panels were 2, 4, and 8 μM for traces 1, 2, and 3, respectively. (*C*) Aggregation of 4 μM rhodanese in the absence (trace 1) or presence of 4 μM wild-type HdeA (trace 2) or 4 μM HdeA(F35K) (trace 3), as monitored by apparent absorbance at 320 nm. Aggregation assays were performed in 100 mM potassium phosphate buffer, 150 mM NaCl (pH 2.2) at 37 °C.

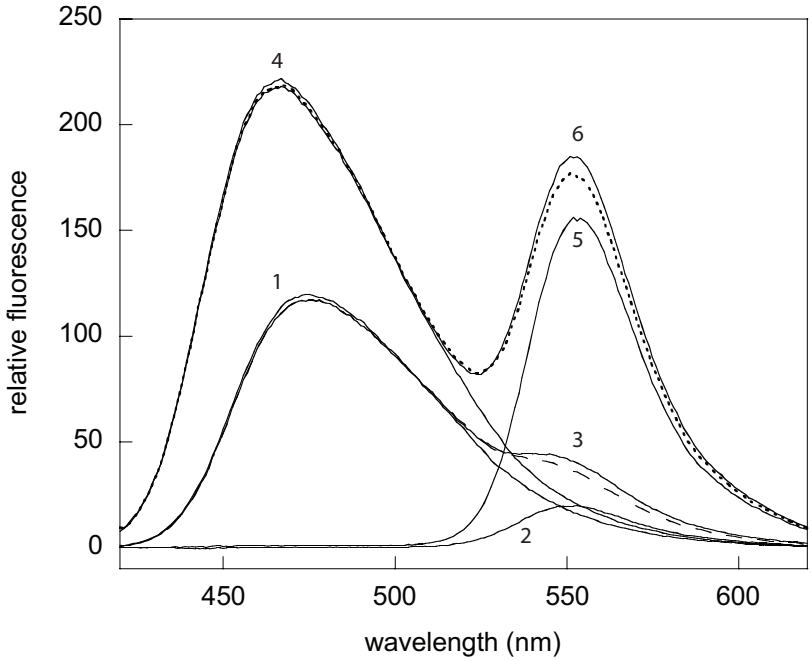

Fig. S7. MDH binding does not induce HdeA oligomerization as indicated by the lack of FRET. Emission spectra of 0.5 μM bimane- (trace 1) or AF532-labeled (trace 2) HdeA(C27), a 1:1 mixture of both (trace 3), or the same spectra as in 1–3 recorded in the presence of MDH [trace 4 is 0.5 μM bimane-labeled HdeA(C27) + 2 μM MDH; trace 5 is 0.5 μM AF532-labeled HdeA(C27) + 2 μM MDH; trace 6 is 1:1 mixture of bimane- and AF532-labeled HdeA(C27) in the presence of 2 μM MDH]. The dashed line is the mathematical sum of traces 1 and 2; the dotted line is the mathematical sum of traces 4 and 5. The considerably large R_0 value (52 Å) for the bimane-AF532 donor–acceptor pair and the lack of any detectable energy transfer suggest that MDH binding does not induce HdeA oligomerization.

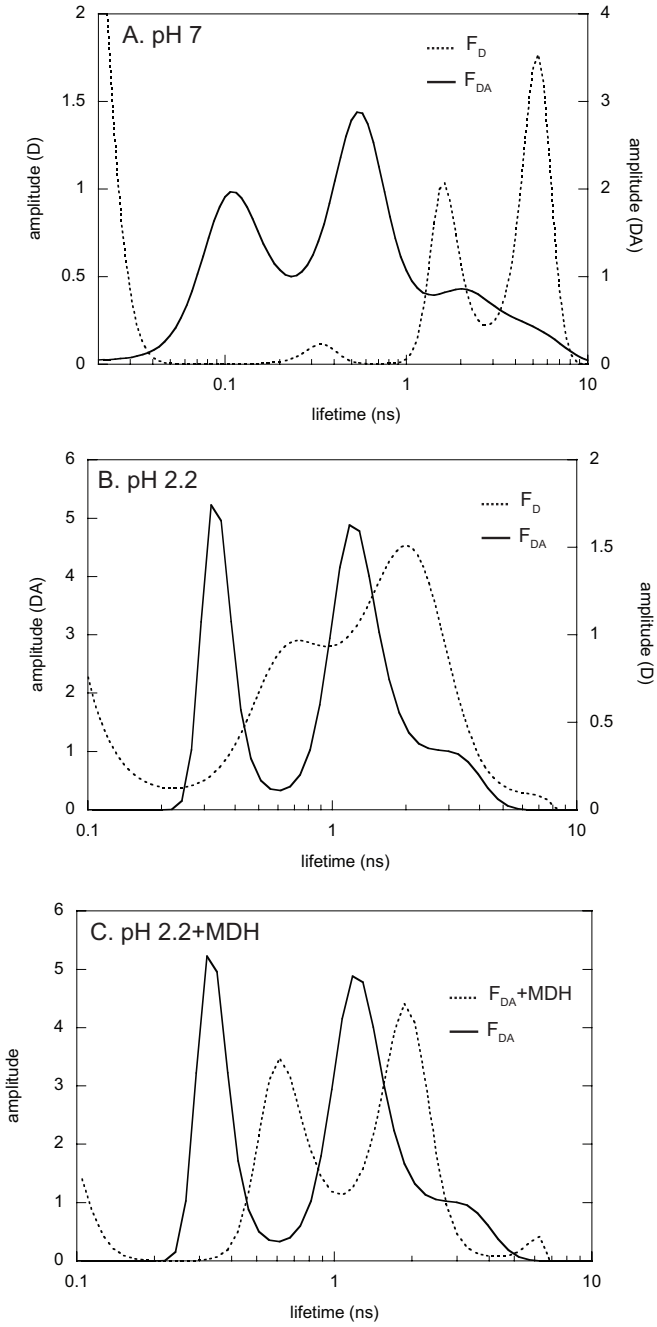

Fig. S8. Maximum entropy method analysis of time-resolved fluorescence of HdeA(W82, C27) in the absence or presence of the TNB quencher at pH 7 (*A*), pH 2.2 (*B*), or at pH 2.2 (*C*) in the presence of bound MDH. The area under each curve represents the concentration of species in each microstate. Average lifetimes and apparent distances are presented in Table S2.

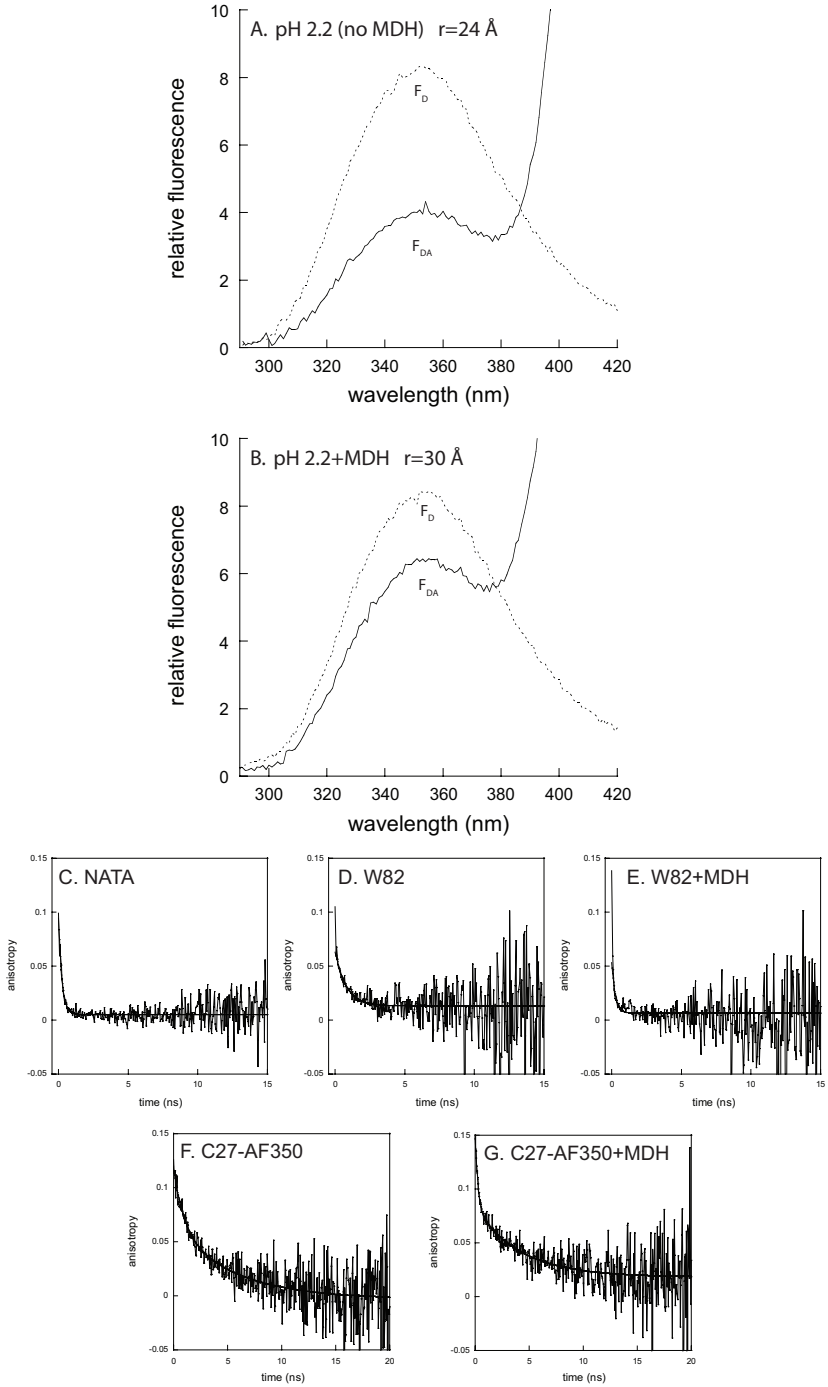

Fig. S9. MDH binding does not increase the apparent distance between the W82 donor and acceptor (attached via C27) through orientation-specific artifacts. Emission spectra of 1 μM unlabeled (F_D, dashed lines) or AF350-labeled HdeA(W82,C27) (F_{DA}, solid lines) at pH 2.2 in the absence (*A*) or in the presence (*B*) of bound MDH (2 μM final concentration). The dramatic increase in fluorescence above 380 nm is caused by acceptor fluorescence; therefore, integrated intensities from 300 to 360 nm were used to calculate FRET efficiency and apparent distances (*r*). (*C*–*G*) Anisotropy decays of the donor (*C*–*E*) and acceptor (*F* and *G*) do not change substantially upon MDH binding. (*C*–*E*) For measurement of donor anisotropy decays, 1 μM NATA (free tryptophan analog (*C*), 1 μM unlabeled HdeA(W82) (*D*), or 1 μM HdeA(W82) in the presence of 2 μM MDH (*E*) was excited at 283 nm, and emission was measured at 340 nm. Decay of donor (W82) fluorescence both the absence and presence of bound MDH was well described a single exponential decay, and the data were fit according to the equation $y = \alpha^{*}e^{(-t/\tau)} + c$, where α is the amplitude and τ is the decay time. Curve fit parameters were: $\alpha = 0.089$, $\tau = 0.24$ ns, and $c = 0.005$ (*C*), $\alpha = 0.05$, $\tau = 0.78$ ns, and $c = 0.012$ (*D*), and $\alpha = 0.05$, $\tau = 0.25$ ns, and $c = 0.006$ (*E*). The complete subnanosecond decay of the donor (W82) anisotropy is similar to that observed for the free tryptophan analog (NATA) in solution, indicating high mobility of the donor. (*F* and *G*) Acceptor anisotropy decays were measured by using 0.5 μM AF350-labeled HdeA(W82,C27) in the absence (*F*) or presence (*G*) of 2 μM MDH. The AF350 was directly excited at 307 nm, and emission was measured at 450 nm. Traces in both *F* and *G* were well described by the sum of two exponential functions and were fit according to the equation $y = \alpha_1{}^{*}e^{(-t/\tau 1)} + \alpha_2{}^{*}e^{(-t/\tau 2)} + c$, where α_1 and τ_1 are the amplitude and decay time of the fast phase and α_2 and τ_2 are the amplitude and decay time of the slow phase. The fast ($<$1 ns) decay phase accounted $\approx$50% of the overall signal in both cases, indicating segmental mobility of the probe in the absence and presence of bound MDH. The following slow component is likely caused by the rotation of the entire protein(s). Curve fit parameters were: $\alpha_1 = 0.055$, $\tau_1 = 0.89$ ns, $\alpha_2 = 0.067$, and $\tau_2 = 5.5$ ns, $c = 0.003$ (*F*) and $\alpha_1 = 0.076$, $\tau_1 = 0.76$ ns, $\alpha_2 = 0.064$, and $\tau_2 = 4.2$ ns, $c = 0.018$ (*G*). All experiments (*A*–*G*) were performed in 100 mM potassium phosphate buffer, 150 mM NaCl (pH 2.2).

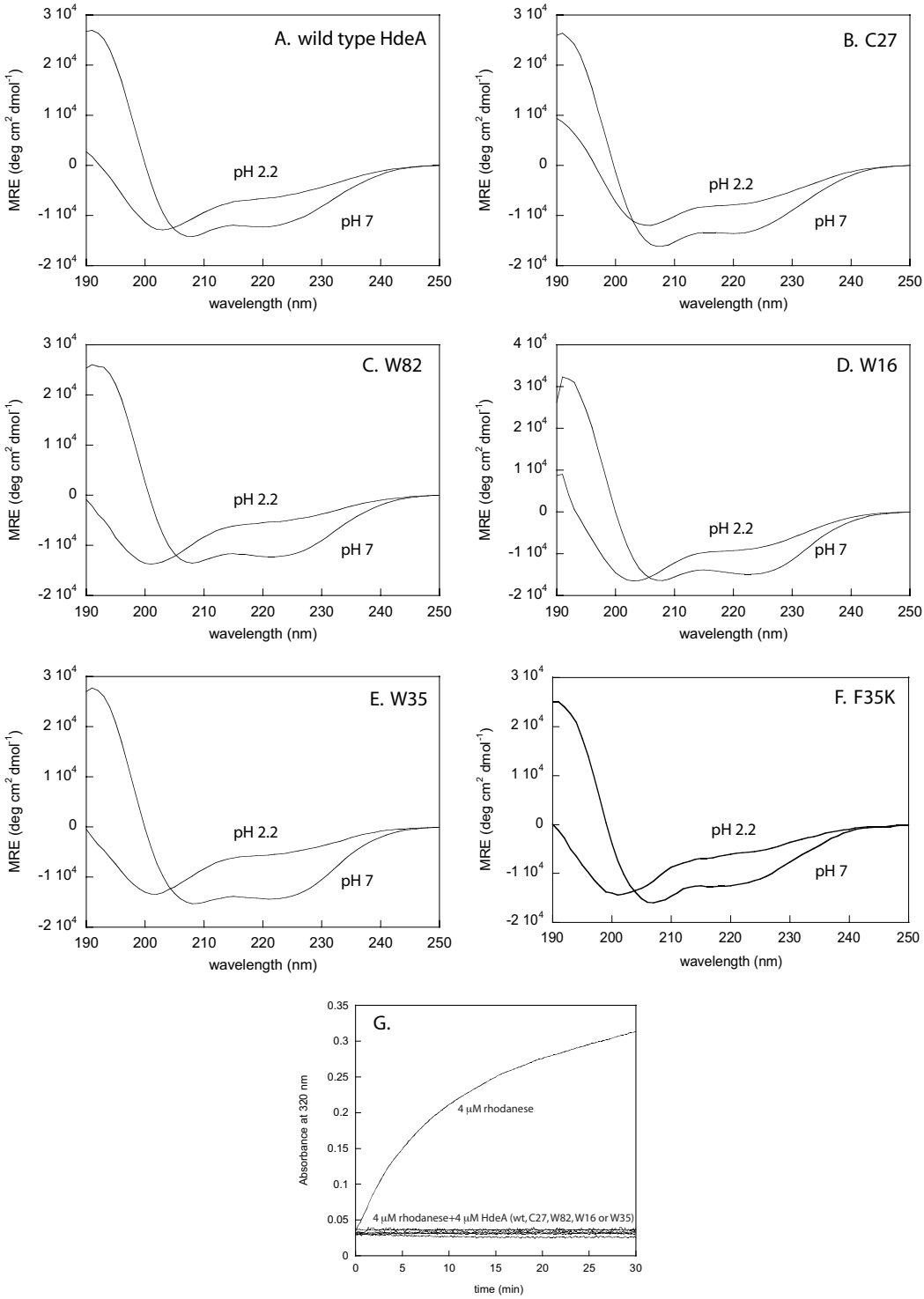

Fig. S10. Structure and activity of HdeA mutants. (*A–F*) Far-UV CD spectra of wild-type HdeA and HdeA mutants. Spectra of 10 μM protein were collected in 10 mM phosphate buffer at pH 7 and pH 2.2 in a 0.1-cm path length quartz cuvette at 23 °C. (*G*) Rhodanese aggregation assays in the absence or presence of wild-type or mutant HdeA. Assays were performed by diluting Gdn-denatured rhodanese to a final concentration of 4 μM into 100 mM phosphate buffer (pH 2.2) + 150 mM NaCl. For experiments in the presence of HdeA, a final concentration of 4 μM wild-type HdeA, HdeA(W16), HdeA(W82), HdeA(W35), or HdeA(C27) was included in the buffer before addition of rhodanese. Aggregation was monitored by following apparent changes in absorbance caused by light scatter at 320 nm in a Cary100 spectrophotometer equipped with Peltier temperature control set to 23 °C. In each case, addition of HdeA resulted in a suppression of rhodanese aggregation, indicating that each mutant exhibits chaperone-like activity.

Table S1. Nomenclature used in the text for HdeA variants

HdeA protein	Position(s) of Trp residues	Nomenclature used in text
Wild-type HdeA	16, 82	Wild-type HdeA
W16F	82	HdeA(W82)
W82L	16	HdeA(W16)
W16F/W82L	None	Trp-less HdeA
W16F/W82L/F35W	35	HdeA(W35)
S27C	16, 82	HdeA(C27)
W16F/S27C	82	HdeA(W82,C27)

Wild-type refers to the mature HdeA protein from *E. coli* (National Center for Biotechnology Information accession number NP_417967).

Table S2. Summary of fluorescence lifetime data presented in Fig. S8

	pH 7		pH 2.2		
Parameter	TNB (DA)	Cleaved (D)	TNB (DA)	Cleaved (D)	TNB + MDH (DA + substrate)
τ (ns)	Av = 0.36	Av = 3.68	Av = 0.92	Av = 1.65	Av = 1.45
	Long = 0.545	Long = 5.23	Long = 1.25	Long = 2.03	Long = 1.85
	Short = 0.115	Short = 1.60	Short = 0.34	Short = 0.72	Short = 0.64
E_T	Av = 0.915	xx	Av = 0.46	xx	Av = 0.1
	Long = 0.9		Long = 0.39		Long = 0.09
	Short = 0.93		Short = 0.53		Short = 0.11
r (Å)	Av = 17.0	xx	Av = 21.0	xx	Av = 29.4
	Long = 17.5		Long = 22.0		Long = 30.0
	Short = 16.4		Short = 20.0		Short = 28.9

τ, fluorescence lifetime. E_T, energy transfer efficiency. *r*, donor to acceptor distance calculated from E_T and R_0 = 25.2 Å at pH 7 and R_0 = 20.4 Å at pH 2.2.